Helmholtz-Zentrum Dresden-Rossendorf (HZDR)

HZDR
HELMHOLTZ ZENTRUM
DRESDEN ROSSENDORF

Defect characterization using positron annihilation spectroscopy on laser ablated surfaces

Hosemann, P.; Auguste, R.; Lam, S.; Butterling, M.; Liedke, M. O.; Elsherif, A. G. A.; Hirschmann, E.; Wagner, A.; Grigoropoulos, C. P.; Selim, F.; Uberuaga, B. P.;

Originally published:

October 2021

JOM: The Journal of the Minerals, Metals & Materials Society 73(2021), 4221-4230

DOI: https://doi.org/10.1007/s11837-021-04965-8

Perma-Link to Publication Repository of HZDR:

https://www.hzdr.de/publications/Publ-33184

Release of the secondary publication
on the basis of the German Copyright Law § 38 Section 4.

Defect characterization using positron annihilation spectroscopy on laser ablated surfaces.

P. Hosemann[12*], R. Auguste[1], S. Lam[1], M. Butterling[3], M. O. Liedke[3], A. G. Attallah[3], E. Hirschmann[3], A. Wagner[3], C. P. Grigoropoulos[4], F. Selim[5], B. P. Uberuaga[6]

*Corresponding author, peterh@berkeley.edu

[1]*Nuclear Engineering, University of California, Berkeley, Berkeley, USA*

[2]*Lawrence Berkeley National Laboratory, Berkeley, USA*

[3] *Helmholtz-Zentrum Dresden - Rossendorf, Institute of Radiation Physics, Bautzner Landstraße 400, 01328 Dresden, Germany*

[4] *Mechanical Engineering, University of California, Berkeley, Berkeley, USA*

[2]*Bowling Green state university, Ohio, USA*

[3]*Los Alamos National Laboratory, Los Alamos, NM, CA, USA*

Abstract:

In recent years, short, pulsed laser ablation has been gaining popularity for machining small scale test geometries from bulk samples and for efficient serial sectioning. These laser-based techniques are being added to the toolbox in material science, which makes it necessary to understand the changes in the material that occur from the laser-material interaction. Positron annihilation spectroscopy is a unique, nondestructive technique to investigate small defects in materials difficult to investigate by other tools. In this work, Doppler broadening and positron lifetime annihilation spectroscopy are utilized to help quantify the damage in materials treated with short, pulsed lasers. Using a femtosecond laser on single crystal silicon, this manuscript shows that clusters of vacancy-like defects and small voids increase systematically with laser power. The damage induced by the laser can also reach to micrometer depths.

Introduction:

Generating and preparing structures at the mesoscale has been a challenging task, be it for device fabrication and the mechanical tensile test samples, or even microscopy samples. Preparing structures at the length scale of <100 µm is usually done using conventional high-speed machining, grinding, polishing, and similar techniques. Macro and micro electrical discharge machining (EDM) is one popular approach and can remove large amounts of material and manufacture complicated geometries. Of course, all these methods leave surface damage and one may state that, the larger the material removal rate, the greater the surface damaging that will occur simply due to the fact that more heat is generated or more deformation needs to occur [1, 2]. Smaller sample preparation and geometries are created either via chemical processes and lithography which involves fab facilities and carry a high entry hurdle. Alternatively, ion beam-based processing allows for the creation of complicated structures with minimal damage on virtual any kind of material [2, 3]. However, these processes tend to be rather slow and time consuming. The large time commitment for focus ion beam (FIB) processing is currently addressed by automation and digital image correlation to compensate for drift while still obtaining accurate cutting. Processing speed is overcome with plasma FIB systems that utilize ions with higher sputter yield and high currents. However, most FIB machines are costly to purchase and maintain [4].

Nuclear materials have the added challenge that they are radioactive, and any material removed from the surface is highly radioactive. The debris or waste can easily contaminate vacuum chambers while radioactive liquid acid waste is a challenge to treat. FIB materials processing contaminates the vacuum system and as more material is removed the more contamination piles up, leading to highly contaminated FIB systems.

A solution to this challenge is utilizing laser fabrication techniques since the physical ablation can be separated from the environment [5]. Laser processing has the advantage that it can be done through glass windows and can physically separate the radioactive area from the environment and the laser source. Therefore, laser ablation machining is a leading technique for working on radioactive materials and reactor retrieved components.

Other applications of femtosecond laser ablation include surface patterning to create hydrophobic surfaces. In fact, surface engineering to reduce the contact angle between a liquid and a solid may alter the corrosion properties of a material and enhance the component lifetime [6].

However, with reduced sample size and surface patterning, surface damage becomes more of an issue and one must consider the surface damage the laser causes. Previous studies examined the damage caused by femtosecond laser ablation using transmission electron microscopy (TEM) [5] and surface scanning electron microscopy (SEM) and optical microscopy [7, 8]. It was found that the near-surface damage reaches as far as a micrometer in depth using TEM. However, the onset of damage as a function of laser energy and damage depth, particularly comparing the laser damage to conventional surface prepared samples, has not been examined. Furthermore, the point vacancy-type defects cannot be detected using optical or electron microscopy techniques. Positron annihilation spectroscopy (PAS), however can detect the atomic scale vacancy type defects generated in the early stages of damage before they become visible for TEM. The focus of this work is to investigate these types of defects that contribute to the surface damage but may not be visible in TEM at low laser power.

In this work, we set out to investigate these types of defects that contribute to the surface damage but may not be visible in TEM at lower laser power.

Experimental:

Single crystal silicon wafers were used to produce the samples. The manufacturer provided 3" diameter Si wafers which had a single side mirror polished. The silicon wafer was cut into several 1cm x 1cm coupons. One coupon remained as received while one coupon was ground with 600 grit SiC paper effectively making the polishing quality of the surface worse than the as received condition. It is estimated that this grinding step removed <25μm of surface material. Three additional coupons were surface treated with a femtosecond laser. The laser system utilizes a *Spectra-Physics Spirit One 8W* femtosecond laser manipulated by a *Newport* manufacturing center equipped with a 2.5 axis stage. The laser during the machining process operated with a pulse width of 332 fs, a repetition rate of 200 kHz, a wavelength of 1040 nm, and an approximate spot size of 10 μm. Air flow positioned on the surface of the sample was used to remove excess ablation. The

entire surface of each Si sample was scanned with a single set of horizontal lines, which were spaced 4 μm apart and therefore had overlapping paths. In total, 3 samples were produced with this method at varying system powers of 0.0145 W, 0.145 W and 0.29 W. This leads to 73 nJ, 725 nJ and 1.5 μJ of beam energy per pulse leading to as much as 92 mJ/cm^2 on the low energy sample and 1.8 J/cm^2 on the high energy sample considering the 10 μm diameter beam spot. The resulting surfaces are shown in Figure 1.

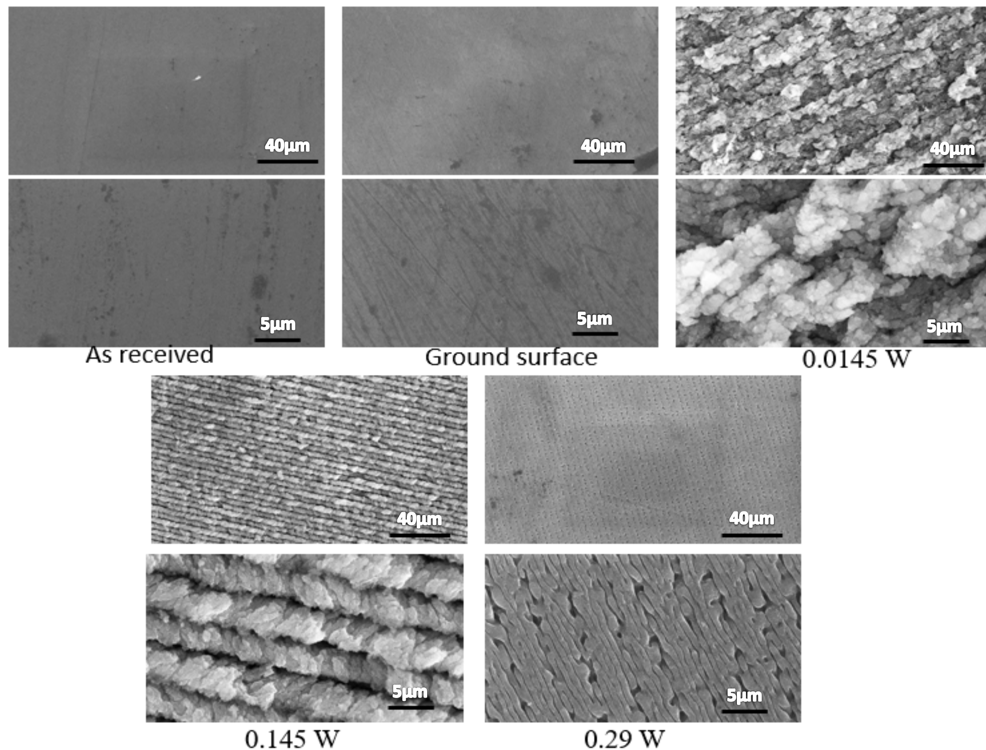

Figure 1: SEM images of silicon as prepared via the different methods displaying at two different magnifications.

The samples were investigated using PAS to characterize the damage at different depths at the user facility at the Helmholtz-Zentrum Dresden - Rossendorf (HZDR). Doppler broadening variable energy positron annihilation spectroscopy (DB-VEPAS) measurements have been conducted at the apparatus for in-situ defect analysis (AIDA) [9] of the slow positron beamline (SPONSOR) [10]. Positrons were implanted into each sample with discrete kinetic energies E_p in the range between 0.05 and 35keV, which allows for depth profiling from the surface down to a couple of micrometers. Depth-resolved variable energy positron annihilation lifetime spectroscopy (PALS) was also done to assess the damage at different conditions. Positron implantation energies for each sample include 0.5 - 12 keV in 0.5 keV increments. At these energies, the positrons will probe the

first ~1.6 μm of the samples' thickness (~ 2 × <z>, where <z> is mean positron implantation depth), providing information about the relative defect density at specific depths. [9]

The PALS experiments were performed at the mono-energetic positron source (MePS) beamline, which is one of the end stations of the radiation source ELBE (Electron Linac for beams with high Brilliance and low Emittance) at HZDR (Germany) [11, 12], using a fast $CeBr_3$ scintillator detector coupled to a *Hamamatsu R13089-100* PMT. The PMT has an additional μ-metal shield and is housed inside a solid Au casing. The data acquisition is fully digital utilizing a software employing a *SPDevices ADQ14DC-2X* with 14 bit vertical resolution and 2GS/s horizontal resolution [13] and with a time resolution function down to about 0.205 ns. The resolution function required for spectrum analysis uses two Gaussian functions with distinct intensities depending on the positron implantation energy, E_p, and appropriate relative shifts. All spectra contained at least $1 \cdot 10^7$ counts. Spectra were deconvoluted using the non-linearly least-squared based package PALSfit fitting software [14] into a few discrete lifetime components, which directly reveal different defect types (sizes), and the corresponding relative defect lifetime intensities, which provides relative concentrations of each defect type.

The positron beam penetrating the material is shown in Figure 2. It can be seen that the beam samples the first 1 μm of material depth. A mean positron implantation depth can be approximated (without accounting for diffusion) by a simple material density-dependent, Makhovian positron stopping profile formula [9]: $<z> = 36/\rho \cdot E_p^{1.62}$, where $\rho = 2.329$ g·cm^{-3} (see Fig. 2a). Generally, though, the positron implantation depth profile broadens with increasing implantation energy. [15] After implantation into a solid, positrons lose their kinetic energy due to thermalization and, after a short period of diffusion, annihilate in delocalized lattice sites or localize in vacancy-like defects and interfaces, emitting usually two anti-collinear 511 keV gamma photons after annihilation with the encountered electrons. Since, at the annihilation site thermalized positrons have very small momenta compared to the electrons, a broadening of the 511 keV line is observed mostly due to the momenta of the electrons, which is measured with one or two high-purity Ge detectors (energy resolution of 1.09 ± 0.01 keV at 511 keV) in the framework of Doppler broadening positron annihilation spectroscopy. This broadening is characterized by two distinct line shape parameters S and W, defined as the fraction of the annihilation line in the middle (511 ± 0.70 keV) and outer regions (508.56 ± 0.30 keV and 513.44 ± 0.30 keV) of the spectrum, respectively. The S-parameter

is a fraction of positrons annihilating with low momentum valence electrons and correlates with vacancy-type defects and their concentration. The W-parameter approximates overlap of positron wavefunction with high momentum core electrons and can be utilized to estimate elemental decoration of the annihilation site. [16]

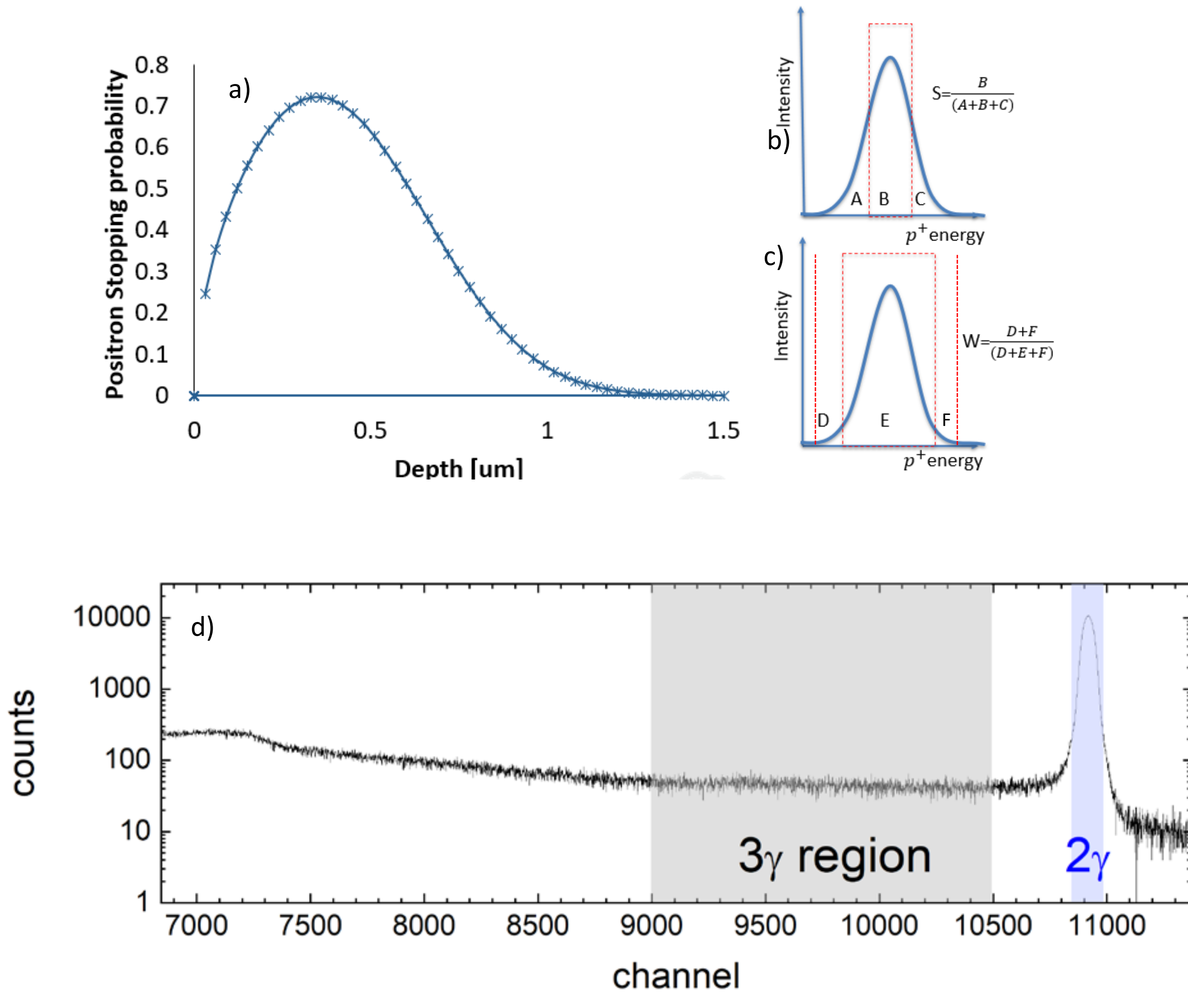

Figure 2: Stopping profile of 14keV positrons in Silicon a). Definition of S parameter and W parameter b) and c). Positron annihilation spectrum labeling 3gamma region and 2gamma region for DB-VEPAS d).

Results and discussion:

FIB X-sections of the laser damaged samples are shown in Figure 3. One can clearly see that the material has deeper damage as a function of laser power. Further the damage manifests itself in the form of pores along the laser path. We can further not distinguish between redeposition debris

and material damage. Furthermore, these images and the PAS measurements are only representative for the same laser and gas flow conditions used in this experiment.

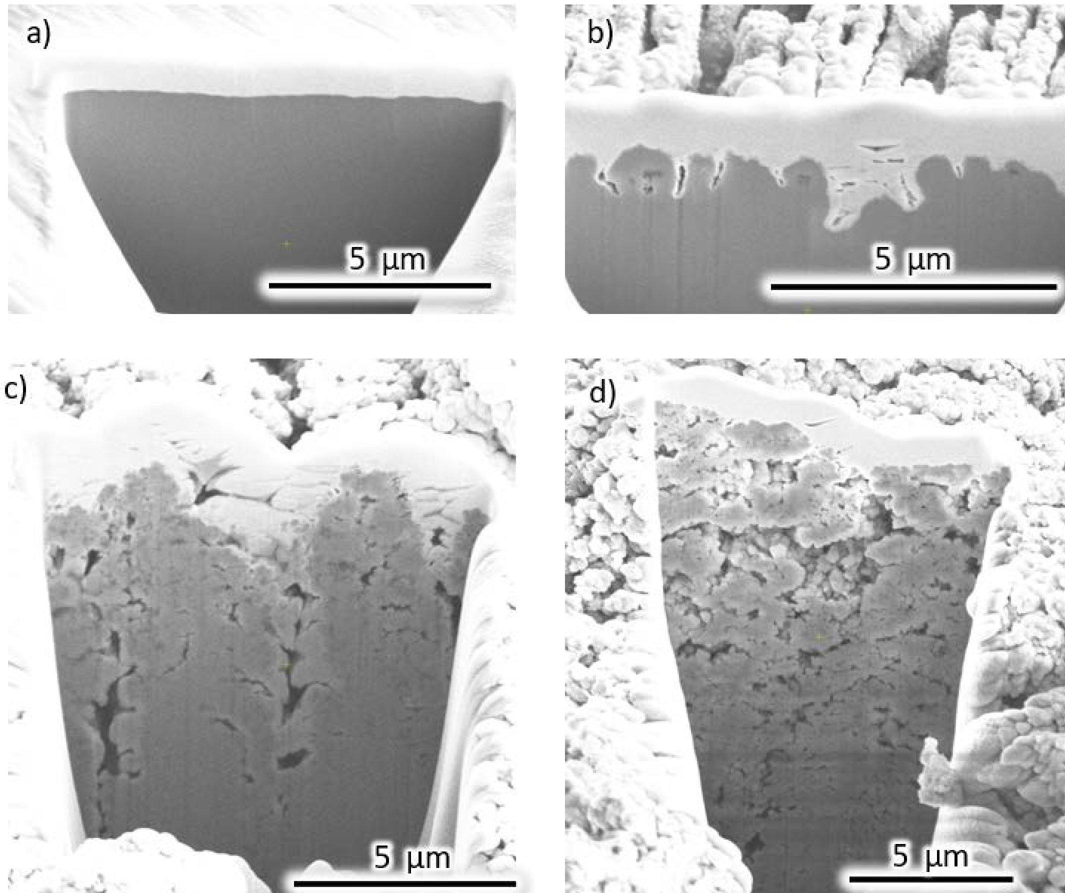

Figure 3: Fib cross section of the as ground Si a), laser treated with 0.0145W b),).145W c) and 0.29W d)

The DB-VEPAS spectra from all five samples are shown in Figure 4. There the S-parameter and W-parameters are shown, revealing depth-dependent information about each sample's defect concentration. The S parameter (low electron momentum fraction; valence electrons) scales proportionally with defect concentration and/or size. The W parameter (high electron momentum fraction; core electrons) indicates the atomic chemistry surrounding the defect [17]. Lastly, 3g2g represents ortho-Positronium (o-Ps) formation, which is generated at surfaces of pores and at the film/vacuum interface. The increased value of the 3/2 gamma ratio suggests enhanced 3 gamma

positron annihilation: o-Ps created at a pore wall diffuses through a pore network and leaves a film to vacuum where it annihilates after ~142 ns. A small fraction of o-Ps will annihilate inside the pore network or large enough isolated pores. Therefore, the samples need to be viewed in relationship to each other: the Si sample, SiC ground sample (rough polished?), and three laser samples need to be compared to draw meaningful conclusions. Figure 4 shows this comparison of S and W-parameter and one can draw the following information from these curves.

The unpolished (as received) sample mirrors commercial Si-substrate: relatively long positron diffusion length L_+ and o-Ps emission at the very surface only. This is very typical for a defect-poor sample. Basically, as a consequence of low defect densities, positrons can more freely diffuse, reaching the surface (back diffusion) or bulk. Typical formation of surface positronium can be seen in Figure 4. The rough polished sample shows much larger open volume in the first 150 nm. However, effects can be seen down to a depth of 1.1 µm within the material. It is obvious that the S-parameter is significantly larger in this region due to the surface preparation. The low energy laser treated sample (0.0145 W) generates open volume complex defects (further discussed in the PALS section of this work) up to a depth of ~600 nm. The elevated 3/2 gamma ratio suggests the formation of porosity. W is similar to the unpolished reference sample, so the sample consists mostly of Si. 0.145 W and 0.29 W generate larger complex defects while the W-parameter changes drastically, becoming more like a mirror reflection of the S parameter, revealing a change in the chemical decoration of the defects; again, the 3/2 gamma ratio suggests increased porosity. The 0.29 W sample exhibits a porous region up to 2 µm in depth and a denser sub-surface region further into the sample (3/2 gamma has a maximum at $E_p = 20$ keV).

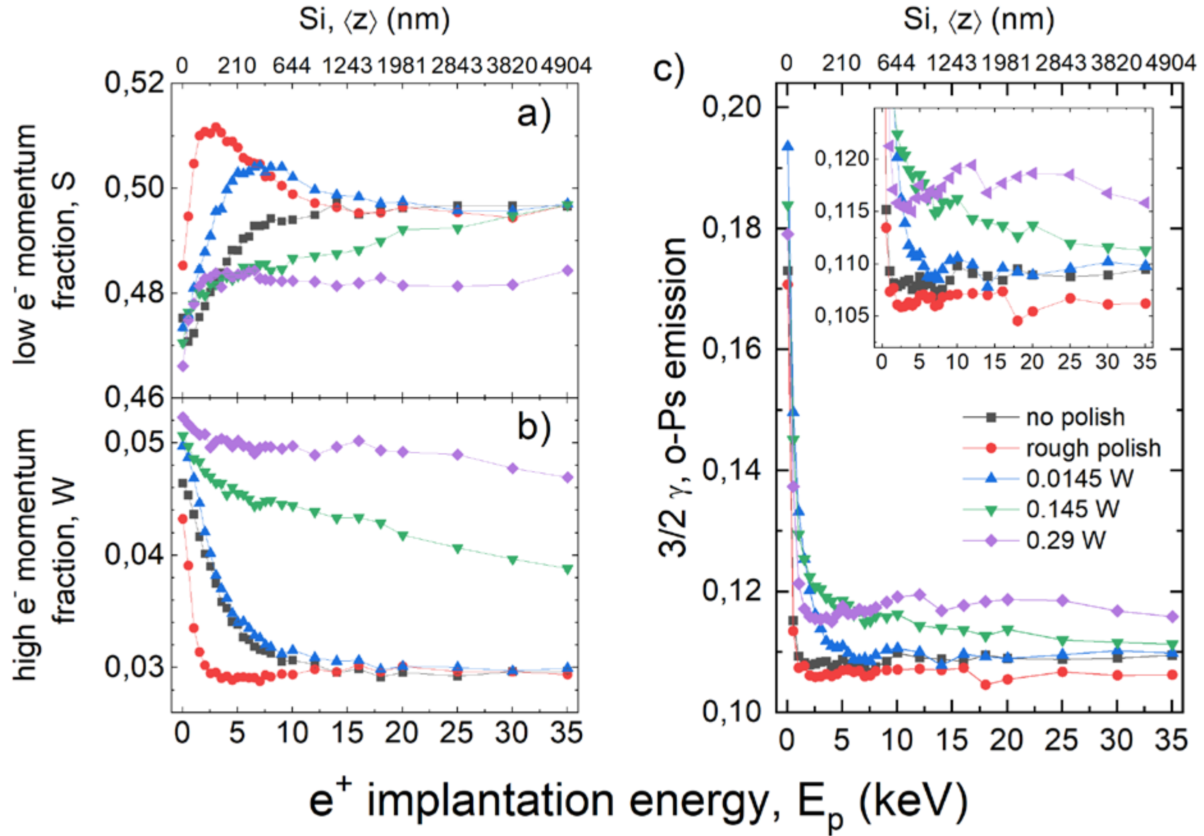

Figure 4: Annihilation line parameter S (low electron momentum fraction) a), W (high momentum fraction) b), normalized 3/2 gamma ratio (o-Ps emission) as a function of positron implantation energy E_p and mean positron implantation depth <z> for c-Si samples c).

In addition to DB-VEPAS, PALS was also conducted at the MePS beamline, HZDR, Germany, to obtain more quantitative information about defect types. With this instrument, the actual lifetime of the positrons is measured. The data are shown in Figure 5. Currently, the positron energy of the beamline is limited to 12 keV and therefore the mean sampled depth that can be investigated is reduced to only 866 nm, as shown. However, one can see tremendous differences between the samples. In addition, since the S-parameter already saturates for E_p above 12 keV, no large changes in positron lifetime are expected for larger energies, too. The average positron lifetime (Figure 5) shows very little difference between the silicon wafer and the rough polished sample, hence similar defect size is expected. Still, τ_{av} of the rough polished sample is slightly larger than the wafer. The reason for the little differences of τ_{av} between both samples, which on the first glance contradict the $S(E_p)$ dependence can be explained by different sensitivity of both parameters: S reflects better the overall defect density, whereas τ_{av} estimates more accurate the defect size. Most likely, the

rough polish introduces a large number of vacancy clusters into the first 50-150 nm below the surface, which signals superimpose with these of the surface states both having positron lifetimes in the similar range (300-500 ps). In case of the silicon wafer mostly surface states are visible. In general, one can see that the higher the laser energy, the longer the average lifetime, indicating significantly larger average open volume size. We will show that the increase of average positron lifetime is an indication of free volume, namely voids and micropores.

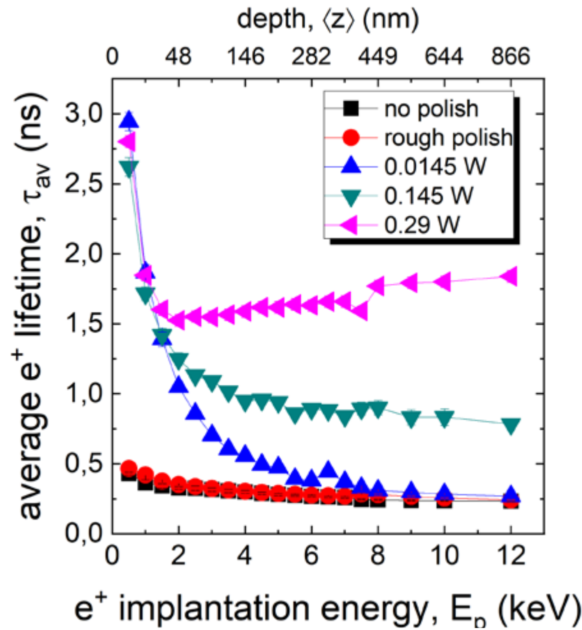

Figure 5: Average positron lifetimes for fs laser Si wafers, obtained from PALS.

As mentioned, the average positron lifetime can be decomposed into its individual constituents, as is described in [17]. The measured spectrum is decomposed according to the fitting equation displayed in Equation 1. Here, τ_n are different lifetime components (Figure 6a) and I_n are their relative intensities (sum is 100 %). The individual lifetimes and intensities are plotted at different lifetime regions, providing more insight into the material's defect structure and properties. Larger open defects, for example, cause an extended lifetime of the positron while larger intensities are caused by more defects.

$$N(t) = I_1 e^{\frac{-t}{\tau_1}} + I_2 e^{\frac{-t}{\tau_2}} + I_3 e^{\frac{-t}{\tau_3}} + I_4 e^{\frac{-t}{\tau_4}} = \sum_n I_n e^{\frac{-t}{\tau_n}} \qquad \text{Equation 1}$$

The decomposition of the PALS data (Fig. 5) exhibits, in general, four annihilation states/defect types. The origins of these lifetime components are:

(i) τ_1 (220-380 ps): e^+ annihilation in bulk, mono- and di-vacancies, and vacancy clusters

(ii) τ_2 (400-1000 ps): e^+ annihilation in larger vacancy clusters (for lifetimes < 500 ps [15]) and Ps annihilation in micropores 1 with d_1<0.4 nm (for lifetimes > 500 ps [18])

(iii) τ_3 (2.5-4.5 ns): Ps annihilation in micropores 2 with d_2<0.7 nm [18]

(iv) τ_4 (8-19 ns): Ps annihilation in micropores 3 with d_3<2.0 nm [18]

The calculation from lifetimes to pore sizes is performed using the shape free model for pore size determination based on the extended Tao-Eldrup model [18]). In every sample, the strong effect of surface states can be seen for positron implantation energies E_p < 2 keV. For that reason, the values discussed in the following for identifying defect types were taken from positron larger energies (where the surface effect is no longer present, and the lifetime and intensity curves flatten or saturate). Lastly, a positron lifetime component can sometimes be found in the PALS data with an intensity dropping towards zero for larger implantation depths (with decreasing influence of the surface). The fit algorithm usually shows this component even if it has intensities less than 1 %. For PALS results, data points with less than 1 % intensity are not shown. The goodness of the 4-components fit (reduced chi-squared) varied from 1.0 to 1.3.

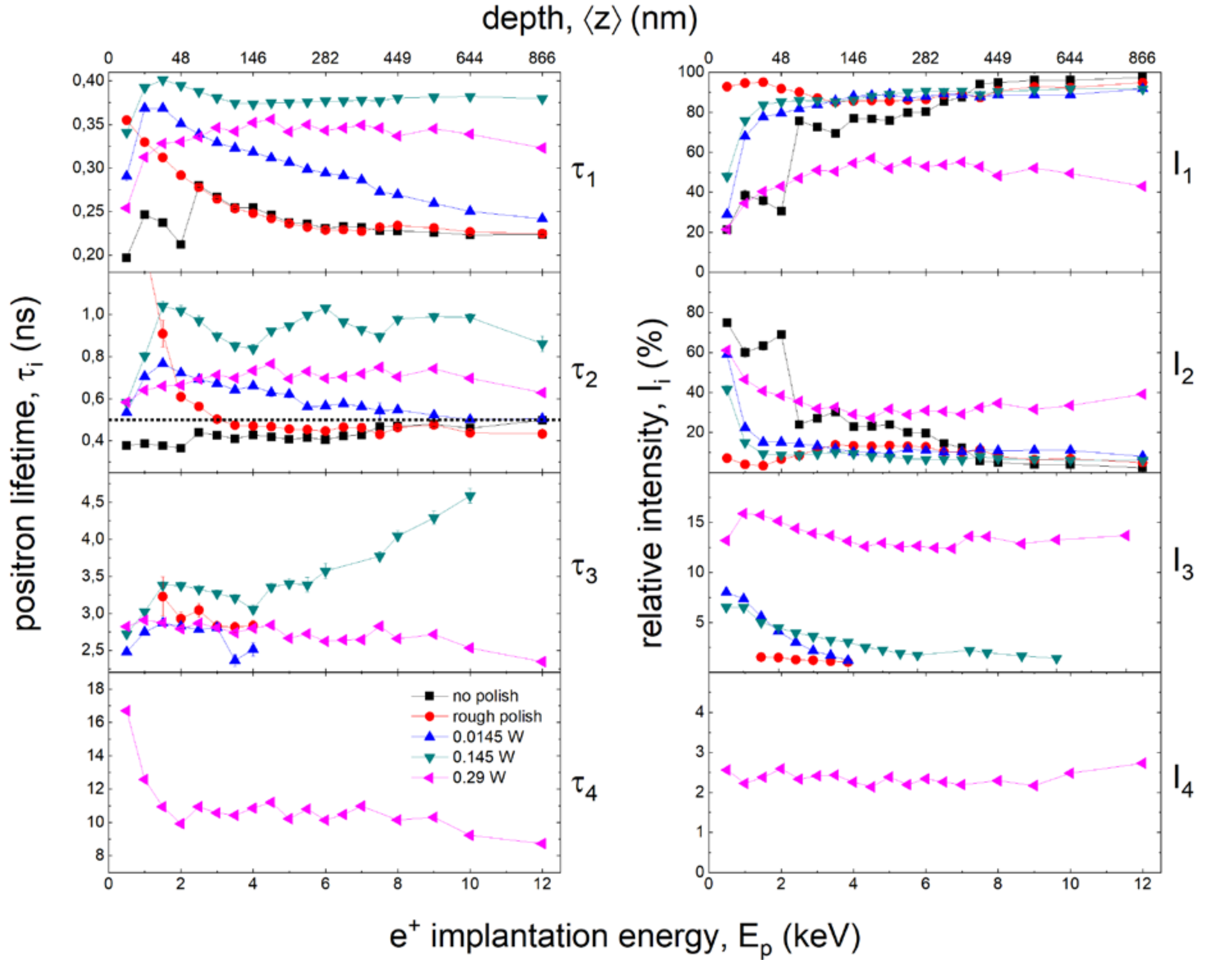

Figure 6: Positron lifetimes (left) and corresponding intensities (right) for the fs laser Si wafers. Data points with less than 1 % intensity are not shown, leading to fewer curves and data points in some of the plots. The horizontal line at 0.5 ns shows the threshold between vacancy clusters and voids/pores [15].

The as-received silicon wafer sample as well as the rough polished sample have a first lifetime value τ_1 approaching 220 ps for larger implantation energies, which is in good agreement with the (defect-free) bulk lifetime value of 218 ps in Si [19]. In contrast, the laser introduces enough defects to increase the overall lifetime values for τ_1 compared to the reference samples. The 0.145 W and 0.29 W samples exhibit increases in τ_1 to ~350 ps and ~380 ps, respectively. For all laser irradiated samples, all positrons annihilate from trapping states indicating high level of defects. However, the size of vacancy clusters and voids enormously increases with increasing laser power. Positron lifetimes in the range <300 ps correspond to mono- and di-vacancies and to larger

complexes [19, 20] as found for the 0.0145 W sample, 5-8 vacancy agglomerations were found for larger laser energies (see ATSUP calculations in Fig. 7 and for example [20]). However, at 0.0145W, the lowest laser energy sample, there is not only an increase in $\tau_1$compared to the reference samples, but also a decrease in τ_1 from 300 ps down to 250 ps bulk Si lifetime as a function of depth, suggesting laser damage in this sample was not deeper than 1 μm. A relatively precise estimation of the laser penetration is given by $S(E_p)$ maximum in Fig. 3.

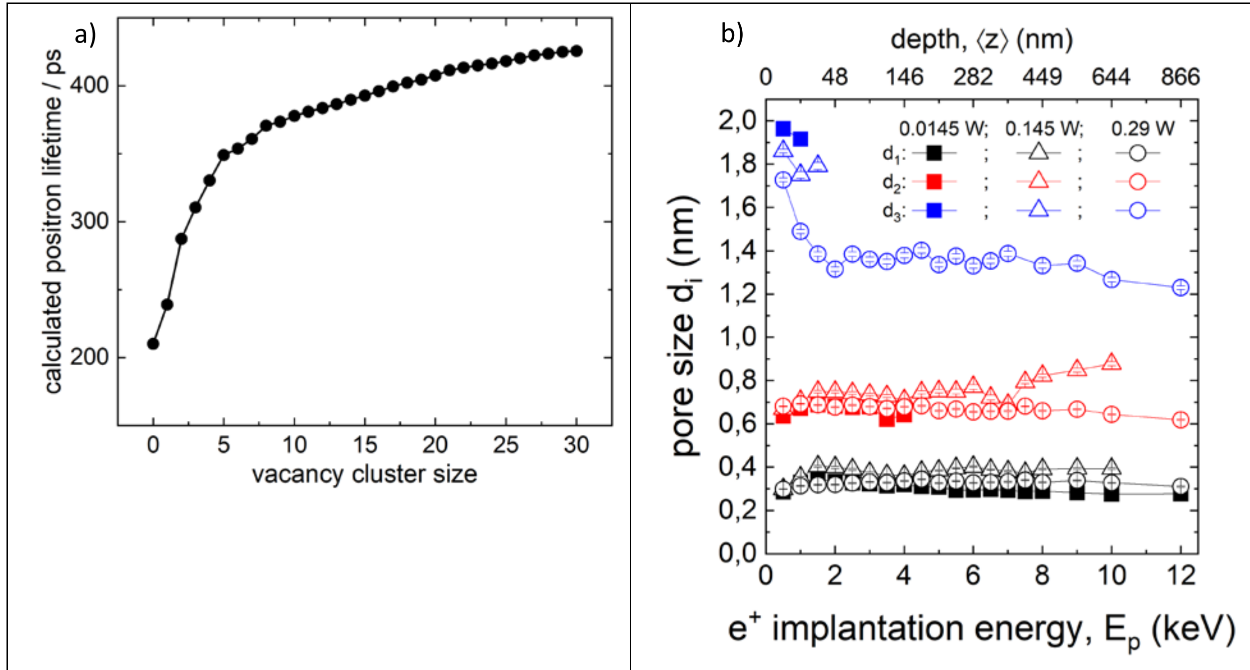

Figure 7: Calculated positron lifetimes on Si crystal using the ATSUP code with BN parametrization (see text) (a). Boronski-Nieminen BN scheme delivers slightly underestimated positron lifetimes compared to [19]. Calculated based on the shape-free model [18] pore sizes for laser annealed samples. (b)

Theoretical calculations of positron lifetimes for the delocalized states (bulk lifetime) and the localized trapped states at defects were obtained by the atomic superposition method (ATSUP) using two-component DFT ab initio calculations [15]. Complex electron-positron interactions are based on a local density approximation (LDA) using a theory for a positron embedded in a homogeneous electron gas. The scheme for electron-positron correlations was used in the frame of the Boronski-Nieminen (BN) [21] approach (taking into account incomplete positron screening).

τ_1 represents a major trapping defect type (with large relative intensity I_1) in all the samples besides the largest laser power, where pore components dominate. The increase in laser energy drives

vacancy agglomeration. Higher laser energies seem to reduce the vacancy content but increases microporosity.

Increasing laser energy leads to an increase in defect lifetime and therefore an increase in vacancy cluster and pore/void size, as can be seen in Figure 6 from the larger lifetime values: τ_2, τ_3, and τ_4. For the unpolished and as-polished reference samples, there the second lifetime component stabilizes to $\tau_2 \approx 450$ ps, which is high enough to be associated with large vacancy-type defect clusters and surface states (see Figure 7 and [19]). The latter are usually in the range of 350-500 ps. Again, the laser enhances defect agglomeration, which is reflected in a rise of the overall lifetime values in τ_2 compared to the reference samples. The 0.145 W and 0.29 W samples show increases in τ_2 to 800-1000 ps and ~700 ps, respectively. The τ_2 value from the lowest laser energy sample shows an overall increase from the reference samples, but again a decrease in τ_2 from 650 ps to 500 ps for deeper energies, further suggesting laser damage in this sample was not as deep as the samples exposed to the higher laser power. As described earlier, positron lifetimes of 800-1000 ps represent the existence of micropores with diameters in the range of d_1 = 0.35 - 0.40 nm [18]. τ_3 and τ_4 are associated with even larger micropores but they are mostly present only for the largest laser energies. For the 0.145 W and 0.29W samples, the τ_3 component is saturated between 2.3 - 4.6 ns (d_2 = 0.62 - 0.88 nm in diameter). The τ_4 component for the 0.29 W sample is mostly between 8.7 - 11 ns (d_3 = 1.2 - 1.4 nm), except in the surface region. Whenever the defect components τ_3 and τ_4 show overall intensity less than 1%, they were not considered significant and have been neglected for clarity.

Two important trends emerge from the PALS lifetime intensity data in Figure 6 after associating τ_2, τ_3, and τ_4 with increasing void size. First, the rough polishing effect seems to cause only slight changes to small vacancy clusters and surface states and no voids are introduced. Rough polishing introduces defects into the sub-surface region, which is evidenced by elevated τ_1 values as compared to the unpolished case. The polished case exhibits a defected sub-surface region (~50 nm) but the overall lifetime is lower compared to the other samples. On the other hand, τ_1 for the unpolished sample likely represents a mixture of surface states (normally 350 - 500 ps) and a small concentration of vacancy clusters (divacancies). The lifetime values at deeper energies look almost identical, which is expected in the case of undamaged bulk. Second, the laser power increases the size of defects and their concentration, especially in case of the largest laser power. The laser-

treated samples show overall increases in defect component lifetimes compared to the reference samples. Even the lowest laser energy sample (0.0145 W) exhibits a small concentration of micropores 1 (pore size d_1, Figure 7b) (with τ_2 representing 8 – 15 % of the overall intensity), in addition to a small population of larger micropores 2 (d_2) occupying mostly the sub-surface region. Irradiation with the 0.29 W laser increases the concentration of the smaller micropores 1 (d_1; I_2 increasing to 27 - 46 % of the overall intensity) and increases the concentration of larger micropores 2 and 3 with average diameters d_2 and d_3 (I_3 and I_4 increasing to ~12 % and ~2 % of the overall intensity, respectively).

Based on the findings highlighted above one can clearly state that the laser surface treatment deployed here leads to significant near-surface changes in the material's microstructure and defect content. Defect structures to a depth of up to 5μm and beyond were found to be present at the higher laser power used here. However, lower powers lead to less deep penetration. This is in agreement with previous studies on Cu and silicon [3, 23] showing that deep damage can occur. In fact, the study here shows that laser power above 0.0145 W leads to damage reaching as deep as 5 μm while lower laser powers only lead to surface damage. Again, the damage appears to be pores and vacancy clusters. We do want to note however, that silicon is particularly more sensitive to damage than most conventional metals and any damage from similar laser treatments is likely significantly less in structural materials.

The experiment here presents works case scenarios with a very limited set of laser scan parameters (90 degree impact, one laser path, limited overlap, limited gas flow, etc). However, this leads to the point that when machining microscale mechanical samples one may need to consider a final cleaning step of the sample surface using ion beam milling or chemical etching to achieve bulk properties.

Conclusions:

Silicon was used to evaluate the impact of different surface preparation methods (grinding and laser treatments) on a material's defect structure and defect development. Surface scanning electron microscopy and positron annihilation spectroscopy methods were used to study these effects.

From positron doppler broadening profiles, positron lifetime values, and intensity depth profiles one can conclude:

- The effect of rough polishing causes only slight changes in the lifetime values. For $E_p < 2$ keV (50 nm), however, the contributions cannot be easily separated from surface annihilation states that have close lifetimes and are dominant in these region, too, due to the limited time resolution of the spectrometer. From DBS, the increased S-parameter shows more open volume from rough polishing, especially in the first 50-150 nm.
- Laser treatment generates complex defects and pores in the entire region. Even for the lowest laser energy, vacancy clusters and small voids are created. The 0.0145 W sample exhibits a pore-rich thickness of about 400 - 500 nm (nicely visualized in Figure 5 where average positron lifetime decays to the values of pristine samples). For larger laser energies, the positron bulk lifetime of 219 ps is no longer visible, indicating that vacancy clusters are generated as deep as a 5μm or deeper. The FIB cross section shows that the damage is indeed dominated by pores and goes beyond the PAS depth.
- The porosity is driven by the laser energy: the larger the energy, the higher the pore concentration and size. Three different pore sizes were found: $d_1 = 0.35 - 0.40$ nm, $d_2 = 0.62 - 0.88$ nm, and $d_3 = 1.2 - 1.4$ nm in diameter. The W-parameter and 3/2 gamma ratio also show increasing porosity with laser power.
- Samples cut using femtosecond laser ablation contain damage and post ion beam cleaning or chemical cleaning must be conducted to remove that damage.
- Materials that have been surface textured with the purpose of creating a surface less prone to corrosion due to wetting will also contain defects that may alter the near-surface mechanical properties. It is also possible that this damage impacts the corrosion in other ways beyond the changes in surface wetting.

Acknowledgement

Research primarily supported as part of FUTURE (Fundamental Understanding of Transport Under Reactor Extremes), an Energy Frontier Research Center funded by the U.S. Department of Energy (DOE). Electron microscopy was performed with the support of the DOE Nuclear Energy University Program (NEUP) for infrastructure. Parts of this research were carried out at

ELBE at the Helmholtz-Zentrum Dresden - Rossendorf e. V., a member of the Helmholtz Association. We would like to thank the facility staff for assistance. This work was partially supported by the Impulse-und Net-working fund of the Helmholtz Association (FKZ VH-VI-442 Memriox), and the Helmholtz Energy Materials Characterization Platform (03ET7015).

Disclaimer:

The authors declare that they have no conflict of interest.

References

[1] Steuer, P., Rebschläger, A., Weber, O., & Bähre, D. (2014). Procedia CIRP, 13, 276–281.

[2] Hejjaji, A., Singh, D., Kubher, S., Kalyanasundaram, D., & Gururaja, S. (2016), 82, 42–52.

[3] J. G. Gigax, H. Vo, Q. McCulloch, M. Chancey, Y. Wang, S. A. Maloy, Nan Li, P. Hosemann, Scripta Mat 170, (2019) 145-149

[4] M.J. Pfeifenberger, M. Mangang, S. Wurster, J. Reiser, A. Hohenwarter, W. Pfleging, D.Kiener, R. Pippan, Mat Design 121 (2017) 109-118

[5] Q. McCulloch, J. G. Gigax, P. Hosemann, JOM **72** (2020) 1694–1702

[6] Tao Liu, Shougang Chen, Sha Cheng, Jintao Tian, Xueting Chang, Yansheng Yin, Elect. Chem. Acta. 52 (2007) 8003-8007

[7] D.V.Tran, H.Y.Zheng, Y.C.Lam, V.M.Murukeshan, J.C.Chai, D.E.Hardt, Optics & Laser engineering 43, (2005) 977-986

[8] N. Ackerl, G. Fisch, J. Auerswald, K. Wegener, SN Applied Science, **2**, (652) (2020)

[9] M.O. Liedke, W. Anwand, R. Bali, S. Cornelius, M. Butterling, T.T. Trinh, A. Wagner, S. Salamon, D. Walecki, A. Smekhova, H. Wende, K. Potzger, J. Appl. Phys. 117 (2015) 163908.

[10] W. Anwand, G. Brauer, M. Butterling, H.R. Kissener, A. Wagner, , Defect Diffus. Forum. 331 (2012) 25–40.

[11] A. Wagner, W. Anwand, A.G. Attallah, G. Dornberg, M. Elsayed, D. Enke, A.E.M. Hussein, R. Krause-Rehberg, M.O. Liedke, K. Potzger, T.T. Trinh, , J. Phys. Conf. Ser. 791 (2017) 012004.

[12] A. Wagner, M. Butterling, M.O. Liedke, K. Potzger, R. Krause-Rehberg, AIP Conf. Proc., 2018: p. 040003.

[13] E. Hirschmann, M. Butterling, U. Hernandez Acosta, M.O. Liedke, A.G. Attallah, P. Petring, M. Görler, R. Krause-Rehberg, A. Wagner, J. Instrum. 16 (2021) P08001.

[14] J. V. Olsen, P. Kirkegaard, N.J. Pedersen, M. Eldrup, Phys. Status Solidi. 4 (2007) 4004–4006.

[15] Puska, M. J., and R. M. Nieminen. 1994. Reviews of Modern Physics 66(3): 841–97.

[16] M. Clement, J.M.M. de Nijs, P. Balk, H. Schut, A. van Veen, J. Appl. Phys. 79 (1996) 9029–9036.

[17] Krause-Rehberg, Reinhard, and Hartmut S Leipner. 1999. Positron Annihilation in Semiconductors: Defect Studies

[18] K. Wada and T. Hyodo Journal of Physics: Conference Series (Vol. 443, No. 1, p. 012003).

[19] M. Saito and A. Oshiyama. 1996. Physical Review B 53(12): 7810–14.

[20] V. Ranki, A. Pelli, and K. Saarinen. 2004. Physical Review B 69(11): 115205..

[21] E. Boroński and R. M. Nieminen (1986) Physical Review B 34 3820

[23] M.S. Rogers, C.P. Grigoropoulos, A.M. Minor, S.S. Mao, Apl. Phys. Let. **94**, (2009), 011111